

Enhancing optical properties of WLEDs with LaOF:Eu³⁺&SiO₂ application

Phuc Dang Huu¹, My Hanh Nguyen Thi²

¹Institute of Applied Technology, Thu Dau Mot University, Binh Duong Province, Vietnam

²Faculty of Mechanical Engineering, Industrial University of Ho Chi Minh City, Ho Chi Minh, Vietnam

Article Info

Article history:

Received Feb 24, 2021

Revised May 20, 2021

Accepted Dec 1, 2021

Keywords:

Dual-layer phosphor

LaOF:Eu³⁺&SiO₂

Mie theory

WLEDs

YAG:Ce³⁺

ABSTRACT

After many efforts, the core-shell nanostructure of LaOF:Eu³⁺&SiO₂ that emits bright red radiation can be fabricated by simple solvothermal application succeeded by heat treatment. The resulted particles from the fabrication process are small in size, able to demonstrate circular form more efficient and prevent stacking. Emissions spectra of photoluminescence (PL) that display strong peaks of 593 nm, 611 nm, and 650 nm are ⁵D₀ → ⁷F_J (J=0, 1 and 2), respectively, Eu³⁺ transitions. Judd-Ofelt (J-O) theory estimates spectral strength parameters and Eu-O ligand behavior. It has been noticed that CIE co-ordinates are very similar to regular NTSC values (x=0.63, y=0.36). Besides, the correlated color temperature value can be observed at below 5000 K, which is 3475 K, and thus it is ideal for warm-light diodes. A fluorescent marker for identification of latent fingerprints was used with the tailored core-shelled SiO₂ (coat III)@LaOF:Eu³⁺ (5 mole %) on porous and non-porous surfaces. The results of fingerprint have high sensitivity, selectivity and also has no obstruction caused by the back-ground which supports level-I to level-III fingerprint ridge recognition. The experiments outcomes suggest that the enhancements brought by the core-shell NS structure can be further examined to apply in forensic and solid state lightning applications.

This is an open access article under the [CC BY-SA](https://creativecommons.org/licenses/by-sa/4.0/) license.



Corresponding Author:

My Hanh Nguyen Thi

Faculty of Mechanical Engineering, Industrial University of Ho Chi Minh City

No. 12 Nguyen Van Bao Street, Ho Chi Minh City, Vietnam

Email: nguyenthimyanh@iuh.edu.vn

1. INTRODUCTION

Regarding efforts to increase the quality of lighting devices, researchers have focused on core-shell structures, which have a number of novel features. There are many models that were applied ranging from hard to soft to create the composition. Despite the variation of models, silica is a material that was consistently used to create core-shell structure because of the changeable dimension [1]-[4]. The core-shell structure fabrication is complete when the layers of shell particles wrapped around the silica centers and generate a spherical core-shell structure. The additional adjustments made to the testing environment and subject production can help achieve non-accumulate circular composition particles. These particles will reduce the light scattering while enhance the intensity and quality of light. In certain fields such as entertainment showcase, bio-medical imaging and anti-counterfeiting applications, these qualities can worth great values [5]-[12]. The rare earth (RE) in composition with nanophosphors can demonstrate acute inception and radiation spectra in UV-Vis region with great amount efficiency, extended working duration, stable chemical composition, heat, and light display, environment friendly and minimal waste. In recent studies, the quantum yield of Sr₄Al₁₄O₂₅ [13]; Ca₁₄Al₁₀Zn₆O₃₅ [14]; CaAl₁₂O₁₉ [15]; Sr₄Al₁₄-O₂₅:Mn⁴⁺, Na⁺,

B^{3+} , $CdGdAlO_4: Pr^{3+}, Yb^{3+}$ [16] is estimated to be 38%, 50%, 35.5%, 60.8% under 450 nm blue light excitation, and 166% respectively [17];. The trivalent luminous lanthanide (Ln^{3+}) ions, which have a comparable ion radius to composite particles, are reasonably easy to mix to the particle configuration and provide good lighting performance even at ambient temperature [18]-[21]. The most notable ion in RE particles' research is Eu^{3+} , which can act as the best material for the creation of red light [22]. Until recently, oxides, phosphates, vanadate, molybdates, borates and fluorides have been proposed as host to add in Eu^{3+} ions. From the doping results, it is confirmed that rare-earth fluorides are the most suitable for integration of various optical active Ln^{3+} ions. The qualities of these substances are high index of refraction, great ionicity low phonon energy, high durability and ionic conductance, resulting in lower non-radiative decay and higher quantum efficiency [23]. The adjustment of exterior layer has resulted in the most changes to the range among luminous and quenching centers, which contribute to the reduction of surface blemishes and non-radiating channels. Regarding all the effects, the core-shell nanostructure is expected to benefit the lighting performance WLEDs [8], [24]. The RE that is integrated with nanomaterials having particle size smaller than 100 nm have been studied especially in latent fingerprints (LFPs) recognition; however, the low fluorescent imaging is the main issue for the application of these materials [25], [26]. Therefore, the importance of innovating an uncomplicated, cost savings, non-detrimental yet precise process to visualize the fluorescent powders of LFPs with features of non-toxicity, high-contrasting chemical and thermal steadiness, super selectivity, minimal interference of background, and high performance in natural environments.

Because of the boundaries pose by the present imaging instrumentation and techniques, LFPs identification is mainly from the primary tool of recognition, analyzing the level II configurations (for example ridge competition, dichotomy, and intersection). The amount of level II properties set must in between 6-17 to ensure the precision of the examination. The problem is the level II configurations on fingertips locate randomly, which demands the size of the finger print images to be large so the result can be more accurate. The LFPs in some cases do not resemble all the properties or missing details after being gathered, which clearly means that factors other than level II of fingerprints must be added to improve the identification process. This need leads to the analyzation of level III structures which has the sweat pore, a persistent trait on the fingertips, unchangeable and distinct, that can improve the result of identification. In current research, researchers developed a core-shell amalgam of $LaOF:Eu^{3+}&SiO_2$ phosphors as a distinctive fluorescent tag for displaying level I to level III crest layouts on various outside platforms. Many researches are being conducted to analyze innovative optical properties or improve performance to apply in more advance usage such as anti-counterfeiting and forensic.

2. PREPARATION AND SIMULATION

2.1. Material preparation

The material preparation process for the composition composes of mixing and firing the components. First, the ingredients are mixing by adding them into water or methanol. Allow the mixture to dry in the air after it has been thoroughly combined, and then crush it into powder. Then prepare a capped quartz tube and fire the mixture at 1000°C for an hour with N_2 . After that, grinding the material chunk into powder before proceeding with the next firing step. Continue to place the powder on capped quartz tube and fire for another hour, this time at 1200°C. After the second firing step, the product is complete and ready to be collected. The obtained material emits red radiation with emission peak at 1.981–2.145 eV. The chemical composition of the compound is presented in Table 1.

Table 1. Chemical composition of $LaOF:Eu^{3+}$

Ingredient	Mole%	By weight (g)
La_2O_3	61 (of La)	99.4
Eu_2O_3	5 (of Eu)	8.8
LaF_3	34	66.6

2.2. Simulation

The LightTools 8.1.0 simulation program as well as the Mie scattering theory are crucial tools for modeling WLEDs with double layers of phosphors. The Mie-principle also enables the investigation of phosphor particle scattering as well as the investigation of $LaOF:Eu^{3+}&SiO_2$ phosphor effects on WLEDs with correlated temperatures ranging from 5600 K to 7000 K. The illustration of the WLED model with specific arrangement of the $LaOF:Eu^{3+}&SiO_2$ and $YAG:Ce^{3+}$ layers is shown in Figure 1. The WLED phosphor package includes the silicone glue, and the two phosphors of $LaOF:Eu^{3+}&SiO_2$ and $YAG:Ce^{3+}$.

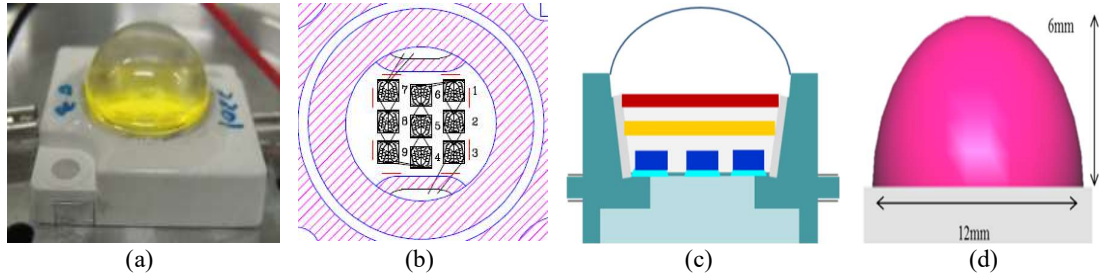


Figure 1. WLEDs structure simulation; (a) the real WLEDs, (b) bonding diagram, (c) demonstration of pc WLEDs structure, and (d) lightTools commercial software based WLEDs model

2.3. Scattering computation

According to Mie scattering theory, the scattered parameter $\mu_{sca}(\lambda)$, anisotropic component $g(\lambda)$, and decreased scattered parameter $\delta_{sca}(\lambda)$ are likely written as the following formulas:

$$\mu_{sca}(\lambda) = \int N(r)C_{sca}(\lambda, r)dr \quad (1)$$

$$g(\lambda) = 2\pi \int_{-1}^1 p(\theta, \lambda, r)f(r)\cos\theta d\cos\theta dr \quad (2)$$

$$\delta_{sca} = \mu_{sca}(1 - g) \quad (3)$$

$N(r)$ denotes the intensity of allocations for spreading phosphor grains (mm^3), C_{sca} denotes the dispersing cross sections (mm^2), $p(\theta, \lambda, r)$ demonstrates the phase purpose, whereas θ , λ , r means respectively the lighting beam wavelength (nm), the diffusional spheres diameter (μm), the dispersing angular position ($^\circ\text{C}$), while $f(r)$ here indicates the diffusional particles scale dispersed ability within WLED's phosphor film. Besides, the $f(r)$ calculation is demonstrated:

$$f(r) = f_{dif}(r) + f_{phos}(r) \quad (4)$$

$$\begin{aligned} N(r) &= N_{dif}(r) + N_{phos}(r) \\ &= K_N[f_{dif}(r) + f_{phos}(r)] \end{aligned} \quad (5)$$

Diffusive and phosphor densities, $N_{dif}(r)$ and $N_{phos}(r)$, are included in $N(r)$. The diffusive and phosphor dimension distribution function values are given by $f_{dif}(r)$ and $f_{phos}(r)$, respectively. K_N is the amount of diffusor units for a specific diffusional-particle concentration and can be measured as:

$$c = K_N \int M(r)dr \quad (6)$$

$M(r)$ denotes the diffusor segment's dispersion volume, which is calculated using the formula:

$$M(r) = \frac{4}{3}\pi r^3 [p_{dif}f_{dif}(r) + p_{phos}f_{phos}(r)] \quad (7)$$

The densities of diffusional ions and phosphorus crystals are represented by $\rho_{dif}(r)$ and $\rho_{phos}(r)$, respectively. By applying the Mie theory, C_{sca} computation is performed as:

$$C_{sca} = \frac{2\pi}{k^2} \sum_0^\infty (2n-1)(|a_n|^2 + |b_n|^2) \quad (8)$$

With $k=2\pi/\lambda$, where the calculation of a_n as well as b_n can be shown as:

$$a_n(x, m) = \frac{\psi_n(mx)\psi_n(x) - m\psi_n(mx)\psi_n(x)}{\psi_n(mx)\xi_n(x) - m\psi_n(mx)\xi_n(x)} \quad (9)$$

$$b_n(x, m) = \frac{m\psi_n(mx)\psi_n(x) - \psi_n(mx)\psi_n(x)}{m\psi_n(mx)\xi_n(x) - \psi_n(mx)\xi_n(x)} \quad (10)$$

With $x=k.r$, while the indicator of refraction is denoted by m , $\psi_n(x)$ together with $\xi_n(x)$ represent the Riccati-Bessel function.

Therefore, the comparative refractive index of diffusional and phosphor particles in silicone, m_{dif} and m_{phos} , may be computed as $m_{dif} = n_{dif}/n_{sil}$ and $m_{phos} = n_{phos}/n_{sil}$, resulting in the phase function computation demonstrated as

$$p(\theta, \lambda, r) = \frac{4\pi(\theta, \lambda, r)}{k^2 C_{sca}(\lambda, r)} \quad (11)$$

In which $\beta(\theta, \lambda, r)$, the angular scattered magnitudes include $S_1(\theta)$ with $S_2(\theta)$ whose computations are shown as the:

$$\beta(\theta, \lambda, r) = \frac{1}{2} [|S_1(\theta)|^2 + |S_2(\theta)|^2] \quad (12)$$

$$S_1 = \sum_{n=1}^{\infty} \frac{2n+1}{n(n+1)} \left[a_n(x, m) \pi_n(\cos\theta) + b_n(x, m) \pi_n(\cos\theta) \right] \quad (13)$$

$$S_2 = \sum_{n=1}^{\infty} \frac{2n+1}{n(n+1)} \left[a_n(x, m) \pi_n(\cos\theta) - b_n(x, m) \pi_n(\cos\theta) \right] \quad (14)$$

With $k_{exi}=462$ nm, the PL spectroscopic radiation density was examined via the similar structure as the item except the concealing sheets. When the covering layer is present in the system, the radiation rate is increased by a factor of three. This effect on the rate of core-shell NS emission contributes to the theory that non-radiative positions on SiO_2 core surfaces are removed by the LaOF:Eu^{3+} shell. The missing surface OH groups in core-shell structure is a result of coating layer on the radiative relaxation pathway. The surface OH groups is still essential to the PL quenching even after the reduction of emission intensity from III coating. Other than the intensities, LaOF:Eu^{3+} & SiO_2 have the equal peak region as well as emission parameters. This result verifies the boosted intensity of LaOF:Eu^{3+} & SiO_2 with NS coating effect of offered by the amorphous silica film, which can be presented as Figure 2.

Figures 2 and 3 show that when SiO_2 is present at 450 nm, the scattering is greater than at 550 nm. This means that the blue light component is dispersed more strongly when SiO_2 is introduced. This boosts luminous flux and improves color homogeneity. The scattering enhances in the phosphor layer, the rays are more uniformly combined, and the resultant color becomes more consistent. The yellow ring phenomena, in other words, is greatly decreased. The blue photons are dispersed more forcefully by the SiO_2 particle, resulting in more light being emitted. These show that the results obtained in section 3 are correct. By using the McCamy imperial equation, the CCT indicators of the un-coated is estimated to be 1854 K and coated sample is 2332 K, which is inadequate for the average lighting requirement of warm white light, see Figure 3.

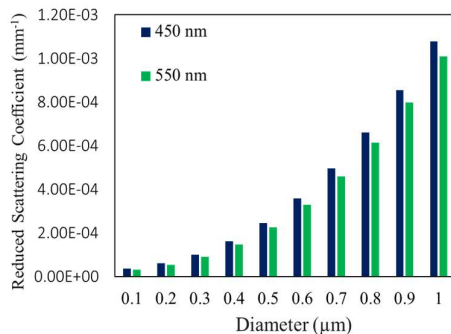


Figure 2. Reduced scattering coefficient of SiO_2 particles at 450 nm and 550 nm

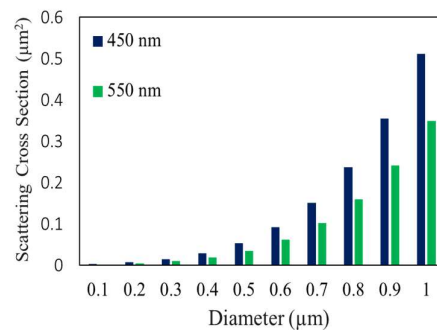


Figure 3. SiO_2 scattered cross-section values

3. RESULTS AND DISCUSSION

Usually, fingerprints (FPs) total ridge patterns can be obtained using a fluorescent powder that was mostly applied when investigating a scene of the crime. The customized LaOF:Eu^{3+} & SiO_2 NS is then discolored on the LFPs that are created from the typical and 254 nm ultra-violet light on a range of hard surfaces, such as metal sheets, aluminum foils, blades, or staplers, to test the quality of the latent FP (LFP) picture collection. Under standard white radiation, the expression of II ridgeline characteristics is optimal;

however, the representation is enhanced by 254 nm ultra-violet lamp. The background interference analysis is conducted by placing tailored LaOF:Eu³⁺&SiO₂ NS upon the porous platforms of outside surroundings such as the newspapers, playing cards, currency note or the covers of several magazines. All of these experimented objects are illuminated with normal white-emitting light and ultra-violet light of 254 nm. FPs results visualized achieved with UV light display have better properties than the other illuminating source. The tailored LaOF:Eu³⁺&SiO₂ NS is also stained beneath white-emitting light and ultra-violet light of 254 nm to investigate more on the specific ridge features of single and over-lapped complex fingerprint pictures. The diversity of level II ridge patterns is fully expressed and without any obstruction in both cases. These outcomes and the content of Figure 4 support the idea that LFPs recognition on porous and non-porous outside surroundings can be performed with optimized powders.

Fluorescent powders performance and different overlapped compound LFPs on the surface of a aluminum foil are verified smearing the LaOF:Eu³⁺&SiO₂ NS illuminated with luminous sources of normal white-emitting light and ultra-violet light of 254 nm. Results from the graph show that viewer can observe ridge details from I-III below usual as well as ultra-violet light of 254 nm. This is the evidence that using phosphor powders with the right adjustment can serve as fluorescent labeling agent to detect fingerprints. In addition, fingerprints from many sources are gathered and applied processed LaOF:Eu³⁺&SiO₂ NS by coating the composite dust below white light like UV light of 254 nm. Each of three prints have different ridges of configurations: center coil, pouch coil, with ulnar arched shape. For a better outcome, high-quality FPs photographs are obtained after a few days of rest. Figure 5 depicts the impacts of LFPs staining on the surface of tinfoil using LaOF:Eu³⁺&SiO₂ NS during a period of 1-9 months. The FPs stains with LaOF:Eu³⁺&SiO₂ NS have excellent consistency for both new and old patterns; the reason for this is due to the high similarity even after ageing latent fingerprints.

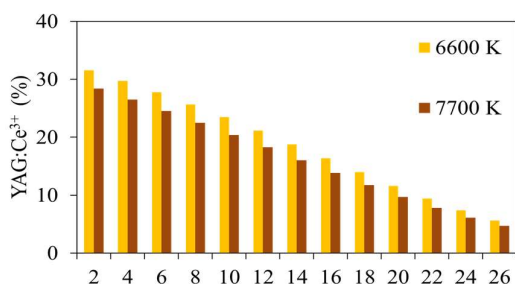


Figure 4. The phosphor concentration fluctuation to maintain the median CCTs

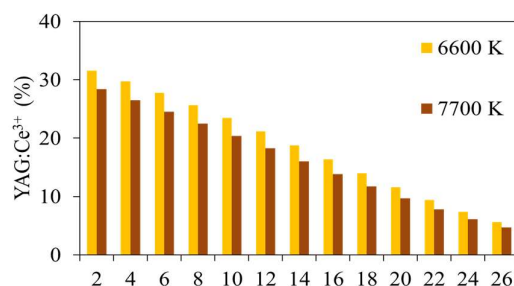


Figure 5. YAG:Ce³⁺ concentration functions as WLEDs colour rendering indicator

The growing pace of research on anticounterfeiting technologies has increased recently to replace conventional methods such as watermarks, holograms, and barcodes, which have become obsolete due to the simplicity of the technique and the risk of being replicated. To strengthen security and deter counterfeit, more advanced technology is being deployed, such as plasmon access controls, biocompatible microscopic handprints, and magnetic sensitivities. Yet, the establishment cost for accurate and modern devices for these methods is counter-intuitive to the safety and cost-saving points of view. Therefore, using the illuminating method to aid the security concern and reduce the cost is the more beneficial option, which is currently being researched for anti-counterfeiting field. The most typical subject for showing luminescent graphics in ultra-violet (UV) illumination is bank notes. Other nanomaterials have been utilized to provide lighting, such as organic dyeing chemical, carbon ions, and semiconducting components; however, waste generation during long-term use or extensive radiation bands prevent this approach from being widely used. The lanthanide-doped nanostructured phosphors, on the other hand, provide outstanding spectral fingerprints with many other desirable properties, such as duplicate proof, low waste emission and high working expectancy has led to their opportunity for employment in anti-counterfeiting field, which can be seen from Figure 6.

The ink's luminous foundation makes it suitable with a wide range of printing devices, including dip-fountain pen written work, printmaking, gravure printing, and letterpress publishing. Figure 7 shows the printed text produced by a dip pen using tailored LaOF:Eu³⁺&SiO₂ NS ink as digital form 254 nm ultra-violet light. The Figure shows distinct and clear images under UV light, which would normally be quite blurry under visible light. The discussed information has proven that LaOF:Eu³⁺&SiO₂ NS are effective and advantageous in many factors if applied to the anti-counterfeiting field.

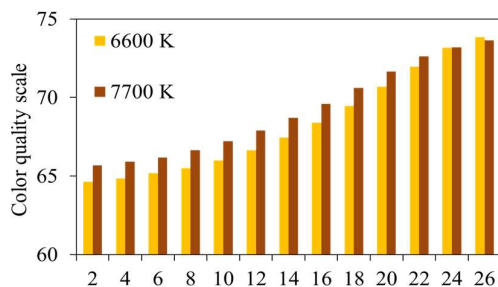


Figure 6. YAG:Ce³⁺ concentration functions as WLEDs colour quality scale

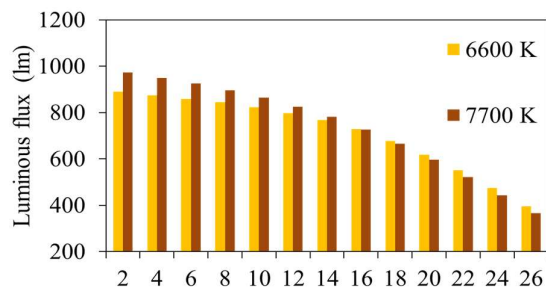


Figure 7. YAG:Ce³⁺ concentration functions as WLEDs illuminating beam

4. CONCLUSION

The solvothermal process was applied for simple and efficient fabrication of the LaOF:Eu³⁺&SiO₂ NS with core-shell structure. After analyzing LaOF:Eu³⁺ with SiO₂ using PXRD, it is confirmed that the maximum value of pure tetragonal phase is at 22L. Under the experiments, the influences of Eu³⁺ concentration on the energy band discrepancy and refractivity were also discovered, although the exact amount is yet to be determined. In the preparation process of the compound, the oxygen disfigurements on the surface were detected from the EPR conclusion. The TEM outcomes confirmed the density of LaOF:Eu³⁺&SiO₂ shell is 8 nm. The NS layer improves the energy transmission of atoms three times by eradicating the captive central area on the surface. The PL enhancement effect is linked to the number of coating layers, with more coating layers means stronger enhancement. The lighting capacity is estimated to increase 56.7% with three layers of LaOF:Eu³⁺&SiO₂ NS shell. The LaOF:Eu³⁺&SiO₂ NS exhibits advanced lighting performance that is sufficient to be used as label factors for LFPs identification on many permeable and semi-permeable object surfaces through dust brushing method. The improved lighting performance comes from the better sticking feature, which allows less air to pass through and oxidizing the compound. The visualization of LFPs using optimized NS achieves greater resolve, more thorough fingerprint ridges, simple light capture, and less rear interference than the current substance used. The subject of this study matter can also be used as a guide to help in anti-counterfeiting applications. Because of its distinct and beneficial properties, core-shell NS is now used in color shows, forensic, and protection systems.





REFERENCES

- [1] S. Feng and J. Wu, "Color lensless in-line holographic microscope with sunlight illumination for weakly-scattered amplitude objects," *OSA Continuum*, vol. 2, pp. 9-16, 2019, doi: 10.1364/OSAC.2.000009.
- [2] Y. Chu *et al.*, "Perception enhancement using importance-driven hybrid rendering for augmented reality based endoscopic surgical navigation," *Biomedical Optics Express*, vol. 9, no. 11, pp. 5205-5226, 2018, doi: 10.1364/BOE.9.005205.
- [3] C. Zhang, L. Xiao, P. Zhong, and G. He, "Photometric optimization and comparison of hybrid white LEDs for mesopic road lighting," *Applied Optics*, vol. 57, no. 16, pp. 4665-4671, 2018, doi: 10.1364/AO.57.004665.
- [4] X. Bao, X. Gu and W. Zhang, "User-centric quality of experience optimized resource allocation algorithm in VLC network with multi-color LED," *Optics Express*, vol. 26, no. 21, pp. 27826-27841, 2018, doi: 10.1364/OE.26.027826.
- [5] Z. Wen *et al.*, "Fabrication and optical properties of Pr³⁺-doped Ba, Sn, Zr, Mg, Ta. O₃ transparent ceramic phosphor," *Optics Letters*, vol. 43, no. 11, pp. 2438-2441, 2018, doi: 10.1364/OL.43.002438.
- [6] Ullah *et al.*, "Household light source for potent photo-dynamic antimicrobial effect and wound healing in an infective animal model," *Biomedical Optics Express*, vol. 9, no. 3, pp. 1006-1019, 2018, doi: 10.1364/BOE.9.001006.
- [7] I. G. Palchikova, E. S. Smirnov, and E. I. Palchikov, "Quantization noise as a determinant for color thresholds in machine vision," *Journal of the Optical Society of America A*, vol. 35, no. 4, pp. B214-B222, 2018, doi: 10.1364/JOSAA.35.00B214.
- [8] A. Keller, P. Bialecki, T. J. Wilhem, and M. K. Vetter, "Diffuse reflectance spectroscopy of human liver tumor specimens - towards a tissue differentiating optical biopsy needle using light emitting diodes," *Biomedical Optics Express*, vol. 9, no. 3, pp. 1069-1081, 2018, doi: 10.1364/BOE.9.001069.
- [9] Z. Li, Y. Tang, J. Li, X. Ding, C. Yan and B. Yu, "Effect of flip-chip height on the optical performance of conformal white-light-emitting diodes," *Optics Letters*, vol. 43, no. 5, pp. 1015-1018, 2018, doi: 10.1364/OL.43.001015.
- [10] C. Huang, Y. Chang, L. Han, F. Chen, S. Li, and J. Hong, "Bandwidth correction of spectral measurement based on Levenberg-Marquardt algorithm with improved Tikhonov regularization," *Applied Optics*, vol. 58, no. 9, pp. 2166-2173, 2019, doi: 10.1364/AO.58.002166.
- [11] P. P. Li *et al.*, "Unveiling of control on the polarization of supercontinuum spectra based on ultrafast birefringence induced by filamentation," *Journal of the Optical Society of America B*, vol. 35, no. 11, pp. 2916-2922, 2018, doi: 10.1364/JOSAB.35.002916.
- [12] Y. Xie *et al.*, "Encapsulated room-temperature synthesized CsPbX₃ perovskite quantum dots with high stability and wide color gamut for display," *Optical Materials Express*, vol. 8, no. 11, pp. 3494-3505, 2018, doi: 10.1364/OME.8.003494.





- [13] C. Zhang, T. Han, S. Cao, X. Cheng, and J. Zing, "Mn⁴⁺-doped fluoride phosphors rapidly synthesized by ball milling," *Optical Materials Express*, vol. 8, no. 1, pp. 73-81, 2018, doi: 10.1364/OME.8.000073.
- [14] Y. Yang, C. Chen, P. Du, X. Deng, J. Luo, W. D. Zhong and L. Chen, "Low complexity OFDM VLC system enabled by spatial summing modulation," *Optics Express*, vol. 27, no. 21, pp. 30788-30795, 2019, doi: 10.1364/OE.27.030788.
- [15] J. Cheng *et al.*, "Luminescence and energy transfer properties of color-tunable Sr₄La₂PO₄3O: Ce³⁺, Tb³⁺, Mn²⁺ phosphors for WLEDs," *Optical Materials Express*, vol. 8, no. 7, pp. 1850-1862, 2018, doi: 10.1364/OME.8.001850.
- [16] F. Chen, K. Chi, W. Yen, J. Sheu, M. Lee and J. Shi, "Investigation on Modulation Speed of Photon-Recycling White Light-Emitting Diodes With Vertical-Conduction Structure," *Journal of Lightwave Technology*, vol. 37, no. 4, pp. 1225-1230, 15 Feb.15, 2019, doi: 10.1109/JLT.2018.2890331.
- [17] X. Li, J. A. Greenberg and M. E. Gehm, "Single-shot multispectral imaging through a thin scatterer," *Optica*, vol. 6, no. 7, pp. 864-871, 2019, doi: 10.1364/OPTICA.6.000864.
- [18] B. Jain *et al.*, "High performance electron blocking layer-free InGaN/GaN nanowire white-light-emitting diodes," *Optics Express*, vol. 28, no. 1, pp. 665-675, 2020, doi: 10.1364/OE.28.000665.
- [19] T. Y. Orudzhev, S. G. Abdullaeva and R. B. Dzhabbarov, "Increasing the extraction efficiency of a light-emitting diode using a pyramid-like phosphor layer," *Journal of Optical Technology*, vol. 86, no. 10, pp. 671-676, 2019, doi: 10.1364/JOT.86.000671.
- [20] S. Sadeghi, B. G. Kumar, R. Melikov, M. M. Aria, H. B. Jalali, and S. Nizamoglu, "Quantum dot white LEDs with high luminous efficiency," *Optica*, vol. 5, no. 7, pp. 793-802, 2018, doi: 10.1364/OPTICA.5.000793.
- [21] H. Jia *et al.*, "High-transmission polarization-dependent active plasmonic color filters," *Applied Optics*, vol. 58, no. 3, pp. 704-711, 2019, doi: 10.1364/AO.58.000704.
- [22] J. Cao, J. Zhang and X. Li, "Upconversion luminescence of Ba₃La₂PO₄3:Yb³⁺-Er³⁺/Tm³⁺ phosphors for optimal temperature sensing," *Applied Optics*, vol. 57, no. 6, pp. 1345-1350, 2018, doi: 10.1364/AO.57.001345.
- [23] E. Chen *et al.*, "Flexible/curved backlight module with quantum-dots microstructure array for liquid crystal displays," *Optics Express*, vol. 26, no. 3, pp. 3466-3482, 2018, doi: 10.1364/OE.26.003466.
- [24] C. Han *et al.*, "Effect of surface recombination in high performance white-light CH₃NH₃PbI₃ single crystal photodetectors," *Optics Express*, vol. 26, no. 20, pp. 26307-26316, 2018, doi: 10.1364/OE.26.026307.
- [25] W. Wang and L. Cai, "On the development of an effective image acquisition system for diamond quality grading," *Applied Optics*, vol. 57, no. 33, pp. 9887-9897, 2018, doi: 10.1364/AO.57.009887.
- [26] Y. Yuan *et al.*, "High luminous fluorescence generation using Ce:YAG transparent ceramic excited by blue laser diode," *Optical Material Express*, vol. 8, pp. 2760-2767, 2018, doi: 10.1364/OME.8.002760.

BIOGRAPHIES OF AUTHORS



Phuc Dang Huu     received a Physics Ph.D. degree from the University of Science, Ho Chi Minh City, in 2018. Currently, He is Research Institute of Applied Technology, Thu Dau Mot University, Binh Duong Province, Vietnam. His research interests include simulation LEDs material, renewable energy. He can be contacted at email: danghuuphuc@tdmu.edu.vn



My Hanh Nguyen Thi     received a Bachelor of Physics from An Giang University, VietNam, Master of Theoretical Physics and Mathematical Physics, Hanoi National University of Education, VietNam. Currently, she is a lecturer at the Faculty of Mechanical Engineering, Industrial University of Ho Chi Minh City, Viet Nam. Her research interests are Theoretical Physics and Mathematical Physics. She can be contacted at email: nguyenthimyanh@iuh.edu.vn